Simultaneous calibration of odometry and sensor parameters for mobile robots

Andrea Censi, *Student Member,* Antonio Franchi, *Member,*
Luca Marchionni, and Giuseppe Oriolo, *Senior Member*

***Abstract*—Consider a differential-drive mobile robot equipped with an on-board exteroceptive sensor that can estimate its own motion, e.g., a range-finder. Calibration of this robot involves estimating six parameters: three for the odometry (radii and distance between the wheels), and three for the pose of the sensor with respect to the robot. After analyzing the observability of this problem, this paper describes a method for calibrating all parameters at the same time, without the need for external sensors or devices, using only the measurement of the wheels velocities and the data from the exteroceptive sensor. Moreover, the method does not require the robot to move along particular trajectories. Simultaneous calibration is formulated as a maximum-likelihood problem and the solution is found in a closed form. Experimental results show that the accuracy of the proposed calibration method is very close to the attainable limit.**

***Index Terms*—Mobile robots, differential-drive, odometry calibration, extrinsic calibration**

I. Introduction

THE operation of a robotic system requires the *a priori* knowledge of the parameters describing the properties and configuration of its sensors and actuators. These parameters are usually divided in *intrinsic* and *extrinsic*. By intrinsic, one usually means those parameters tied to a single sensor or actuator. Examples of intrinsic parameters include the odometry parameters, or the focal length of a pinhole camera. Extrinsic parameters describe the relations among sensors/actuators such as the relative poses of their reference frames.

This paper formulates, analyzes, and solves a calibration problem comprising both the intrinsic odometry parameters of a differential-drive robot *and* the extrinsic calibration between the robot platform and an exteroceptive sensor that can estimate its egomotion. The resulting method can be used to calibrate from scratch all relevant parameters of the most common robotic configuration. No external sensors or prior information are needed. To put this contribution in perspective, we briefly review the relevant literature, starting from the most common approaches for odometry calibration.

A. Censi is with the Control & Dynamical Systems department, California Institute of Technology, 1200 E. California Blvd., 91125, Pasadena, CA. andrea@cds.caltech.edu.

A. Franchi is with the Department of Human Perception, Cognition and Action, Max Plank Institute for Biological Cybernetics, Spemannstraße 44, 72076 Tübingen, Germany. antonio.franchi@tuebingen.mpg.de.

L. Marchionni is with Pal Robotics SL, C/Pujades 77-79, 08005 Barcelona, Spain. luca.marchionni@pal-robotics.com.

G. Oriolo is with the Dipartimento di Informatica e Sistemistica "A. Ruberti", Università di Roma "La Sapienza", via Ariosto 25, I-00185 Rome, Italy. oriolo@dis.uniroma1.it.

A. Related work for odometry calibration

Doebbler *et al.* [1] show that it is possible to estimate the calibration parameters using only internal odometry measurements, if the wheeled platform has enough extra measurements from caster wheels. Most commonly, one resorts to using measurements from additional sensors. For example, Von der Hardt *et al.* show that additional *internal* sensors such as gyroscopes and compasses can be used for odometry calibration [2]. The most popular methods consist in driving the robot along especially crafted trajectories, take some external measurement of its pose by an *external* sensor, and then correct a first estimate of the odometry parameters based on the knowledge of how an error in the estimated parameters affects the final pose. This approach has been pioneered by Borenstein and Feng with the *UMBmark* method [3], in which a differential-drive robot is driven repeatedly along a square path, clockwise and anti-clockwise, taking an external measurement of the final pose; based on the final error, two of the three degrees of freedom in the odometry can be corrected. In the same spirit, Kelly [4] generalizes the procedure to arbitrary trajectories and different kinematics.

An alternative approach is formulating odometry calibration as a filtering problem. A possibility is to use an Extended Kalman Filter (EKF) that estimates both the pose of the robot and the odometry parameters, as shown by Larsen *et al.* [5], Caltabiano *et al.* [6], and Martinelli *et al.* [7]. Foxlin [8] proposes a generalization of this idea, where the filter's state vector contains sensor parameters, robot configuration, and environment map; further research (especially by Martinelli, discussed later) has shown that one must be careful about observability issues when considering such large and heterogeneous systems, as it is not always the case that the complete state is observable.

The alternative to filtering is solving an optimization problem, often in the form of maximum-likelihood estimation. Roy and Thrun [9] propose an on-line method for estimating the parameters of a simplified odometry model for a differential drive robot. Antonelli *et al.* [10], [11] use a maximum-likelihood method for estimating the odometry parameters of a differential-drive robot, using the absolute observations of an external camera. The method is particularly simple because the problem is exactly linear, and therefore can be solved with linear least-squares. Antonelli and Chiaverini [12] show that the same problem can be solved with a *deterministic filter* (a nonlinear observer) obtaining largely equivalent results.

It is worth pointing out some general differences between

the approaches. UMBmark- and EKF-like methods assume that nominal values of the parameters are known a priori, and only relatively small adjustments are estimated. For the EKF, the usual *caveats* apply: the linearization error might be significant, and it might be challenging to mitigate the effect of outliers in the data (originating, for example, from wheel slipping). A nonlinear observer has simpler proofs for convergence and error boundedness than an EKF, but does not provide an estimate of the uncertainty. An offline maximum-likelihood problem has the property that outliers can be dealt with easily, and it is not impacted by linearization, but an *ad hoc* solution is required for each case, because the resulting optimization problem is usually nonlinear and nonconvex.

B. Related work for extrinsic sensor calibration

In robotics, if an on-board sensor is mounted on the robot, one must estimate the sensor pose with respect to the robot frame, in addition to the odometry parameters, as a preliminary step before fusing together odometry and sensor data in problems such as localization and mapping. In related fields, problems of extrinsic calibration of exteroceptive sensors are well studied; for example, calibration of sets of cameras or stereo rigs is a typical problem in computer vision. The problem has also been studied for heterogeneous sensors, such as camera plus (3D) range-finder [13]–[15].

Martinelli and Scaramuzza [16] consider the problem of calibrating the pose of a bearing sensor, and show that the system is not fully observable as there is an unavoidable scale uncertainty. Martinelli and Siegwart [17] describe the observability properties for different combinations of sensors and kinematics. The results are not always intuitive, and this motivated successive works to formally prove the observability properties of the system under investigation.

Mirzaei and Roumeliotis [18] study the calibration problem for a camera and IMU using an Extended Kalman Filter. Hesch *et al.* [19] consider the problem of estimating the pose of a camera using observations of a mirror surface with a maximum-likelihood formulation. Underwood *et al.* [20] and Brookshir and Teller [21] consider the problem of calibrating multiple exteroceptive sensors on a mobile robot.

C. Simultaneous calibration of odometry and exteroceptive sensors

Calibrating odometry and sensor pose at the same time is a chicken-and-egg problem. In fact, the methods used for calibrating the sensor pose assume that the odometry is already calibrated, while the methods that calibrate the odometry assume that the sensor pose is known (or that an additional external sensor is present). Calibrating both at the same time is a more complicated problem that cannot be decomposed in two subproblems.

In [22], we presented the first work (to the best of our knowledge) dealing with the joint calibration of intrinsic odometry parameters and extrinsic sensor pose. In particular, we considered a differential-drive robot equipped with a range-finder, or, in general, any sensor that can estimate its egomotion. This is a very common configuration used in robotics. Later, Martinelli [23] considered the simultaneous calibration of a differential drive robot plus the pose of a *bearing sensor*, a sensor that returns the angle under which a point feature is seen. Mathematically, this is a very different problem, because, as Martinelli shows, the system is unobservable and the pose of the bearing sensor can be recovered only up to scale. Most recently, Martinelli [24] revisits the same problem in the context of a general treatment of estimation problems where the state cannot be fully reconstructed. The concept of *continuous symmetry* is introduced to describe such situations, in the same spirit of "symmetries" as studied in theoretical physics and mechanics (in which often "symmetry" is a synonym for the action of a Lie group), but deriving everything using the machinery of the theory of distributions as applied in nonlinear control theory. Antonelli *et al.* [25] consider the problem of calibrating the odometry together with the intrinsic/extrinsic parameters of an on-board camera, assuming the knowledge of a certain landmarks configuration in the environment.

The method presented in [22] has several interesting characteristics: the robot drives autonomously along arbitrary trajectories, no external measurement is necessary, and no nominal parameters must be measured beforehand. Moreover, the formulation as a static maximum-likelihood problem allows to detect and filter outliers.

The present paper is an extension to that work. With respect to the original paper, we present a nonlinear and a stochastic observability analysis proving that the system is locally observable, as well as a complete characterization of the global symmetries (Section III); more careful treatment of some simplifying assumptions (Section V-B1); more comprehensive experimental data, plus uncertainty and optimality analyses based on the Cramér–Rao bound (Section VI). The additional multimedia materials attached include a C++ implementation and the data files used in the experiements.

II. Problem formulation

Let $\mathrm{SE}(2)$ be the special Euclidean group of planar motions, and $\mathrm{se}(2)$ its Lie algebra [26]. Let $\boldsymbol{q} = (q_x, q_y, q_\theta) \in \mathrm{SE}(2)$ be the robot pose with respect to a fixed world frame (Fig. 1). For a differential-drive robot, the pose evolves according to the differential equation

$$\dot{\boldsymbol{q}} = \begin{pmatrix} \cos q_\theta & 0 \\ \sin q_\theta & 0 \\ 0 & 1 \end{pmatrix} \begin{pmatrix} v \\ \omega \end{pmatrix}. \tag{1}$$

The driving velocity v and the steering velocity ω depend on the left and right wheel velocities ω_L, ω_R by a linear transformation:

$$\begin{pmatrix} v \\ \omega \end{pmatrix} = \boldsymbol{J} \begin{pmatrix} \omega_\mathrm{L} \\ \omega_\mathrm{R} \end{pmatrix}. \tag{2}$$

The matrix $\boldsymbol{J}$ is a function of the parameters r_L, r_R, b:

$$\boldsymbol{J} = \begin{pmatrix} J_{11} & J_{12} \\ J_{21} & J_{22} \end{pmatrix} = \begin{pmatrix} +r_\mathrm{L}/2 & +r_\mathrm{R}/2 \\ -r_\mathrm{L}/b & +r_\mathrm{R}/b \end{pmatrix}, \tag{3}$$

where r_L, r_R are the left and right wheel radius, and b is the distance between the wheels. We assume to be able to measure

the wheel velocities $\omega_{\mathrm{L}}, \omega_{\mathrm{R}}$. We do not assume to be able to *set* the wheel velocities; this method is entirely passive and works with any trajectory, if it satisfies the necessary excitability conditions, outlined in the next section.

We also assume that there is an exteroceptive sensor mounted horizontally (with zero pitch and roll) on the robotic platform. Therefore, the pose of the sensor can be represented as $\boldsymbol{\ell} = (\ell_x, \ell_y, \ell_\theta) \in \mathrm{SE}(2)$ with respect to the robot frame (Fig. 1). Thus, at any given time t, the pose of the sensor in the world frame is $\boldsymbol{q}(t) \oplus \boldsymbol{\ell}$, where "$\oplus$" is the group operation on $\mathrm{SE}(2)$. The definitions of "$\oplus$" and the group inverse "$\ominus$" are recalled in Table I.

The exteroceptive observations are naturally a discrete process $\boldsymbol{m}^k$: observations are available at a set of time instants $t_1 < \cdots < t_k < \cdots < t_n$, not necessarily equispaced in time. Consider the generic k-th interval $t \in [t_k, t_{k+1}]$. Let the initial and final pose of the robot be $\boldsymbol{q}^k = \boldsymbol{q}(t_k)$ and $\boldsymbol{q}^{k+1} = \boldsymbol{q}(t_{k+1})$. Denote by $\boldsymbol{s}^k$ the displacement of the sensor during the interval $[t_k, t_{k+1}]$; this corresponds to the motion between $\boldsymbol{q}^k \oplus \boldsymbol{\ell}$ and $\boldsymbol{q}^{k+1} \oplus \boldsymbol{\ell}$ (Fig. 1) and can be written as

$$\boldsymbol{s}^k = \ominus \left(\boldsymbol{q}^k \oplus \boldsymbol{\ell}\right) \oplus \left(\boldsymbol{q}^{k+1} \oplus \boldsymbol{\ell}\right).$$

Letting $\boldsymbol{r}^k = \ominus \boldsymbol{q}^k \oplus \boldsymbol{q}^{k+1}$ be the robot displacement in the interval, the sensor displacement can be also written as

$$\boldsymbol{s}^k = \ominus \boldsymbol{\ell} \oplus \boldsymbol{r}^k \oplus \boldsymbol{\ell}. \tag{4}$$

We assume that it is possible to estimate the sensor's egomotion $\boldsymbol{s}^k$ given the exteroceptive measurements $\boldsymbol{m}^k$ and $\boldsymbol{m}^{k+1}$, and we call $\hat{\boldsymbol{s}}^k$ such estimate (for example, if the sensor is a range-finder, the egomotion can be estimated via scan matching).

At this point, the problem to be solved can be stated formally.

Problem 1. *(Simultaneous calibration)* Given the wheel velocities $\omega_{\mathrm{L}}(t)$, $\omega_{\mathrm{R}}(t)$ for $t \in [t_1, t_n]$, and the estimated sensor egomotion $\hat{\boldsymbol{s}}^k$ $(k = 1, \ldots, n-1)$ corresponding to the exteroceptive observations at times $t_1 < \cdots < t_k < \cdots < t_n$, find the maximum likelihood estimate for the parameters $r_{\mathrm{L}}, r_{\mathrm{R}}, b, \ell_x, \ell_y, \ell_\theta$.

III. Observability analysis

It has become (good) praxis in robotics to provide an observability analysis prior to solving an estimation problem. Usually this is a proof that the system is locally weakly observable [27] according to nonlinear observability theory. It is required that the system is in the continuous-time form

$$\begin{aligned} \dot{\boldsymbol{x}} &= \boldsymbol{f}(\boldsymbol{x}, \boldsymbol{u}), \\ \boldsymbol{y} &= \boldsymbol{g}(\boldsymbol{x}), \end{aligned} \tag{5}$$

where $\boldsymbol{x}$ contains both parameters and time-varying state, and $\boldsymbol{y}$ are continuous-time observations. Such analysis does not take into account the uncertainty in the observations. This analysis is performed in Section III-A.

The alternative is a stochastic analysis based on the Fisher Information Matrix [28], which assumes that the system is in the static form

$$\boldsymbol{y} = \boldsymbol{h}(\boldsymbol{x}, \boldsymbol{u}) + \boldsymbol{\epsilon}, \tag{6}$$

Table I
Symbols used in this paper

calibration parameters to be estimated

$r_{\mathrm{R}}, r_{\mathrm{L}}$	wheel radii
b	distance between wheels
$\boldsymbol{\ell}$	sensor pose relative to robot frame

Robot kinematics

$\boldsymbol{q}$	robot pose relative to world frame
$\omega_{\mathrm{L}}, \omega_{\mathrm{R}}$	left/right wheel velocity
v, ω	driving/steering robot velocities
$\boldsymbol{J}$	linear map between wheel and robot velocities

Sensing process

$\boldsymbol{m}^k$	exteroceptive measurements, available at time t_k
$\boldsymbol{r}^k$	robot displacement in the k-th interval $[t_k, t_{k+1}]$
$\boldsymbol{s}^k$	sensor displacement in the k-th interval
$\hat{\boldsymbol{s}}^k$	sensor displacement estimated from $\boldsymbol{m}^k$ and $\boldsymbol{m}^{k+1}$
$\boldsymbol{\nu}$	sensor velocity in the sensor frame

Other symbols

$\oplus, \ominus$ "$\oplus$" is the group operation on $\mathrm{SE}(2)$:

$$\begin{pmatrix} a_x \\ a_y \\ a_\theta \end{pmatrix} \oplus \begin{pmatrix} b_x \\ b_y \\ b_\theta \end{pmatrix} = \begin{pmatrix} a_x + b_x \cos(a_\theta) - b_y \sin(a_\theta) \\ a_y + b_x \sin(a_\theta) + b_y \cos(a_\theta) \\ a_\theta + b_\theta \end{pmatrix}$$

"$\ominus$" is the group inverse:

$$\ominus \begin{pmatrix} a_x \\ a_y \\ a_\theta \end{pmatrix} = \begin{pmatrix} -a_x \cos(a_\theta) - a_y \sin(a_\theta) \\ +a_x \sin(a_\theta) - a_y \cos(a_\theta) \\ -a_\theta \end{pmatrix}$$

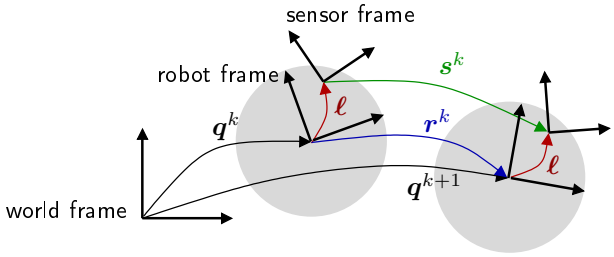

Figure 1. The robot pose is $\boldsymbol{q}^k \in \mathrm{SE}(2)$ with respect to the world frame; the sensor pose is $\boldsymbol{\ell} \in \mathrm{SE}(2)$ with respect to the robot frame; $\boldsymbol{r}^k \in \mathrm{SE}(2)$ is the robot displacement between poses; and $\boldsymbol{s}^k \in \mathrm{SE}(2)$ is the displacement seen by the sensor in its own reference frame.

where $\boldsymbol{y}$ is now a vector of discretized observations and $\boldsymbol{\epsilon}$ is additive stochastic noise. The system is said to be observable if the Fisher information matrix of $\boldsymbol{x}$ is full rank, when $\boldsymbol{u}$ is chosen appropriately. This analysis is presented in Section III-B; its discretized character better captures the nature of our calibration problem, which is naturally discretized by the availability of the exteroceptive observations.

The two analyses give consistent results. Note, however, that both are *local*, in the sense that they cannot account for global symmetries of the parameter space; we discuss such symmetries in Section III-C.

A. Nonlinear/continuous observability analysis

To perform this analysis, the system must be put in the form (5), where the state $\boldsymbol{x}$ includes both the robot pose $\boldsymbol{q}$ and the calibration parameters. This causes two problems. Firstly, (5) is a continuous differential equation with a continuous observation process $\boldsymbol{y}$. This implies that one has to approximate the estimation of sensor pose displacement given two successive measurements—a naturally *discrete* process—by an equivalent *continuous* observation. Secondly, including

the robot pose $\boldsymbol{q}$ as part of the state vector makes the observability analysis hopeless, because the pose $\boldsymbol{q}$ in the world frame cannot be observed from the relative measurements $\boldsymbol{m}$; using the terminology of [24], the system has a continuous symmetry that spans all components of the pose $\boldsymbol{q}$. We show how both problems are solved at the same time.

We need to find a continuous-time analogous of the discrete-time sensor egomotion $\boldsymbol{s}^k$ in the interval $[t_k, t_{k+1}]$. We note that, as the interval between measurements tends to zero, the sensor displacement tends to the sensor *velocity*. Thus, we assume that, in the context of a nonlinear observability analysis, we can abstract the processing of the exteroceptive measurements as a relative velocity sensor.

Denote the sensor velocity in the sensor frame by $\boldsymbol{\nu} = (\nu_x, \nu_y, \nu_\theta) \in \mathrm{se}(2)$. By simple algebra (or by general-purpose frame-to-frame transformations [26]), it can be shown that $\boldsymbol{\nu}$ depends on the sensor pose and the robot velocities:

$$\begin{aligned} \begin{pmatrix} \nu_x \\ \nu_y \end{pmatrix} &= \boldsymbol{R}(-\ell_\theta) \left[\begin{pmatrix} v \\ 0 \end{pmatrix} + \begin{pmatrix} 0 & \omega \\ -\omega & 0 \end{pmatrix} \begin{pmatrix} \ell_x \\ \ell_y \end{pmatrix} \right], \\ \nu_\theta &= \omega. \end{aligned} \tag{7}$$

Here, $\boldsymbol{R}(\cdot)$ represents a 2×2 rotation matrix. This expression does not depend on the robot pose $\boldsymbol{q}$; this is intuitive, as the velocity seen by the sensor does not depend on the absolute robot pose in the world frame. It is also significant, because we can remove the pose $\boldsymbol{q}(t)$ from the observability analysis (it is not observable itself, and it does not influence the observations of the observable parameters). Thus, in this case, a nonlinear observability analysis leads to a degenerate model that lacks any dynamics, and for which observability is easily proved.

Proposition 2. *According to a nonlinear continuous-time observability analysis of the static observation model (7), if $r_\mathrm{L}, r_\mathrm{R}, b \neq 0$, the calibration parameters are observable from the measurements obtained from two trajectories with linearly independent constant wheel velocities.*

Proof: The observations (7) can be written as a linear function of ω_L, ω_R:

$$\boldsymbol{\nu} = \boldsymbol{\nu}_\mathrm{L}(\boldsymbol{x})\, \omega_\mathrm{L} + \boldsymbol{\nu}_\mathrm{R}(\boldsymbol{x})\, \omega_\mathrm{R},$$

where $\boldsymbol{x} = (r_\mathrm{L}, r_\mathrm{R}, b, \ell_x, \ell_y, \ell_\theta)$ contains all parameters to be estimated, and $\boldsymbol{\nu}_\mathrm{L}, \boldsymbol{\nu}_\mathrm{R}$ are given by

$$\boldsymbol{\nu}_\mathrm{L}(\boldsymbol{x}) = \begin{pmatrix} +(J_{11} + \ell_y J_{21}) \cos \ell_\theta - \ell_x J_{21} \sin \ell_\theta \\ -(J_{11} + \ell_y J_{21}) \sin \ell_\theta + \ell_x J_{21} \cos \ell_\theta \\ J_{21} \end{pmatrix},$$

$$\boldsymbol{\nu}_\mathrm{R}(\boldsymbol{x}) = \begin{pmatrix} +(J_{12} + \ell_y J_{22}) \cos \ell_\theta - \ell_x J_{22} \sin \ell_\theta \\ -(J_{11} + \ell_y J_{22}) \sin \ell_\theta + \ell_x J_{22} \cos \ell_\theta, \\ J_{22} \end{pmatrix}.$$

By choosing the two canonical trajectories $(\omega_\mathrm{L}, \omega_\mathrm{R}) = (1, 0)$ and $(\omega_\mathrm{L}, \omega_\mathrm{R}) = (0, 1)$, we obtain the observations vector

$$\boldsymbol{y} = [\boldsymbol{\nu}_\mathrm{L}(\boldsymbol{x})^T \ \boldsymbol{\nu}_\mathrm{R}(\boldsymbol{x})^T]^T, \tag{8}$$

The system is locally observable if the Jacobian $\partial \boldsymbol{y} / \partial \boldsymbol{x} = [\partial \boldsymbol{\nu}_\mathrm{L} / \partial \boldsymbol{x} \ \ \partial \boldsymbol{\nu}_\mathrm{R} / \partial \boldsymbol{x}]$ is full rank. A few simple algebraic steps (omitted) show that the determinant of the Jacobian is $-r_\mathrm{L}^2 r_\mathrm{R}^2 / b^5$, therefore it is nonsingular assuming $r_\mathrm{L}, r_\mathrm{R}, b \neq 0$. The result is unchanged if any other two linearly independent trajectories are chosen. ∎

B. Linearized/discrete observability analysis

To apply this analysis, we should put the system in the static form (6), where $\boldsymbol{x}$ are the states to be estimated, $\boldsymbol{y}$ are the observations, and $\boldsymbol{\epsilon}$ is additive noise. In the next sections, we will use this form to introduce quantitative bounds for the accuracy of the estimated parameters on a given trajectory using the Cramér–Rao bound. For now, we are only interested in showing that the parameters are observable: this can be done by showing that the map $\boldsymbol{h}$ in (6) is a local diffeomorphism.

Proposition 3. *According to a stochastic discrete-time observability analysis of the model (4), if $r_\mathrm{L}, r_\mathrm{R}, b \neq 0$, the calibration parameters are observable from the measurements obtained from two trajectories with linearly independent constant wheel velocities.*

Proof: This analysis uses the actual nonlinear model, and the observations are the displacements $\boldsymbol{s}^k$ given by (4). Suppose the robot moves with constant wheel velocities in the interval $[t_k, t_{k+1}]$. Let the corresponding constant velocity in the sensor frame be $\boldsymbol{\nu}^k \in \mathrm{se}(2)$. Using elementary Lie group theory, we can write the displacement $\boldsymbol{s}^k$ as the solution at time $T^k = t_{k+1} - t_k$ of the differential equation $\dot{\boldsymbol{s}}(t) = \boldsymbol{s}(t)\boldsymbol{\nu}$, with the initial condition $\boldsymbol{s}(0) = \boldsymbol{0}$. The solution can be written as $\boldsymbol{s}^k = \mathrm{Exp}(T^k \boldsymbol{\nu}^k)$, where Exp is the exponential map from $\mathrm{se}(2)$ to $\mathrm{SE}(2)$.

As before, choose the two canonical trajectories $(\omega_\mathrm{L}, \omega_\mathrm{R}) = (1, 0)$ and $(\omega_\mathrm{L}, \omega_\mathrm{R}) = (0, 1)$ and suppose we only consider one observation for each trajectory with equal interval T. The observation vector is $\boldsymbol{y} = [\mathrm{Exp}(T\, \boldsymbol{\nu}_\mathrm{L}(\boldsymbol{x}))^T \ \ \mathrm{Exp}(T\, \boldsymbol{\nu}_\mathrm{R}(\boldsymbol{x}))^T]^T$. Compare this with (8), which is the equivalent under the continuous-time approximation, which, instead of the poses (in $\mathrm{SE}(2)$), observes the velocities (in $\mathrm{se}(2)$).

Stochastic observability is preserved by regular changes of coordinates. We choose to do the change of coordinates $\tilde{\boldsymbol{y}} = \mathrm{Exp}^{-1}(\boldsymbol{y})/T$. This is a diffeomorphism for small motions (the map is not invertible for motions larger than $180°$). We obtain the fictional observations $\tilde{\boldsymbol{y}} = [\boldsymbol{\nu}_\mathrm{L}(\boldsymbol{x})^T \ \boldsymbol{\nu}_\mathrm{R}(\boldsymbol{x})^T]^T$, which are formally the same as (8). We have already shown that the Jacobian $\partial \tilde{\boldsymbol{y}} / \partial \boldsymbol{x}$ is full rank. Thus the Fisher information matrix has full rank, and all parameters are observable. The result is unchanged if any other two linearly independent trajectories are chosen. ∎

C. Global ambiguities

The two analyses presented have only *local* validity: they assert that it is possible to distinguish the true solution from its neighbors, but they do not account for global symmetries in the parameter space. By inspection, we find one such global symmetry.

Proposition 4. *The two sets of calibration parameters $(r_\mathrm{L}, r_\mathrm{R}, b, \ell_x, \ell_y, \ell_\theta)$ and $(-r_\mathrm{L}, -r_\mathrm{R}, -b, -\ell_x, -\ell_y, \ell_\theta + \pi)$ are indistinguishable.*

Proof: By substitution in (7), they give the same sensor velocity, and therefore the same observations. ∎

By convention, we will choose the solution with $b > 0$, so that b has the physical description of the (positive) distance between the wheels.

We can also show that that there are no other symmetries.

Proposition 5. *There is no other global symmetry, other than the one described by Proposition 4.*

Proof: The proof is "constructive" in the sense that it is based on the analysis of the calibration method. In particular, we will show that the solution to the maximum-likelihood problem has a unique solution, after the symmetry of Proposition 4 is taken into account. ∎

IV. Maximum-likelihood formalization of the calibration problem

Formulating the problem as a maximum-likelihood problem means seeking the parameters that best explain the measurements, and involves deriving the objective function (the measurement log-likelihood) as a function of the parameters and the measurements.

Consider the robot motion along an arbitrary configuration trajectory $\boldsymbol{q}(t)$ with observations at times $t_1 < \cdots < t_k < \cdots < t_n$. Consider the k-th interval, in which the robot moves from pose $\boldsymbol{q}^k = \boldsymbol{q}(t_k)$ to pose $\boldsymbol{q}^{k+1} = \boldsymbol{q}(t_{k+1})$. The robot pose displacement is $\boldsymbol{r}^k = \ominus \boldsymbol{q}^k \oplus \boldsymbol{q}^{k+1}$. This quantity depends on the wheel velocities $\omega_{\mathrm{L}}(t)$, $\omega_{\mathrm{R}}(t)$, for $t \in [t_k, t_{k+1}]$, as well as the odometry parameters. To highlight this dependence, we write $\boldsymbol{r}^k = \boldsymbol{r}^k(r_{\mathrm{L}}, r_{\mathrm{R}}, b)$. We also rewrite equation (4), which gives the constraint between $\boldsymbol{r}^k$, the sensor displacement $\boldsymbol{s}^k$, and the sensor pose $\boldsymbol{\ell}$, evidencing the dependence on the odometry parameters:

$$\boldsymbol{s}^k = \ominus \boldsymbol{\ell} \oplus \boldsymbol{r}^k(r_{\mathrm{L}}, r_{\mathrm{R}}, b) \oplus \boldsymbol{\ell}. \tag{9}$$

We assume to know an estimate $\hat{\boldsymbol{s}}^k$ of the sensor displacement, distributed as a Gaussian[1] with mean $\boldsymbol{s}^k$ and known covariance $\boldsymbol{\Sigma}_k$. The log-likelihood $\mathcal{J} = \log p(\{\hat{\boldsymbol{s}}^k\} | r_{\mathrm{L}}, r_{\mathrm{R}}, b, \boldsymbol{\ell})$ is

$$\mathcal{J} = -\tfrac{1}{2} \sum_{k=1}^{n} ||\hat{\boldsymbol{s}}^k - \ominus \boldsymbol{\ell} \oplus \boldsymbol{r}^k(r_{\mathrm{L}}, r_{\mathrm{R}}, b) \oplus \boldsymbol{\ell}||^2_{\boldsymbol{\Sigma}_k^{-1}}, \tag{10}$$

where $||\boldsymbol{z}||^2_{\boldsymbol{A}} = \boldsymbol{z}^T \boldsymbol{A} \boldsymbol{z}$ is the $\boldsymbol{A}$-norm of a vector $\boldsymbol{z}$. We have reduced calibration to an optimization problem.

Problem 6. *(Simultaneous calibration, maximum-likelihood formulation)* Maximize (10) with respect to $r_{\mathrm{L}}, r_{\mathrm{R}}, b, \ell_x, \ell_y, \ell_\theta$.

This maximization problem is nonconvex; therefore, it cannot be solved efficiently by general-purpose numerical techniques [29]. However, we can still solve it in a closed form, according to the algorithm described in the next section.

[1]We treat $\mathrm{SE}(2)$ as a vector space under the assumption that the error of $\hat{\boldsymbol{s}}^k$ is small. More precisely, the vector space approximation is implicit in stating that the distribution of $\hat{\boldsymbol{s}}^k$ is Gaussian, and, later, in equation (10) when writing the norm of the difference $\|\boldsymbol{a} - \boldsymbol{b}\|_{\boldsymbol{A}}$ for $\boldsymbol{a}, \boldsymbol{b} \in \mathrm{SE}(2)$.

V. Calibration method

This section describes an algorithmic solution to Problem 6. The method is summarized as Algorithm 1 on the following page.

The algorithm provides the exact solution to the problem, if the following technical assumption holds.

Assumption 1. *The covariance $\boldsymbol{\Sigma}_k$ of the estimate $\hat{\boldsymbol{s}}^k$ is diagonal and isotropic in the x and y direction:*

$$\boldsymbol{\Sigma}_k = diag((\sigma^k_{xy})^2, (\sigma^k_{xy})^2, (\sigma^k_\theta)^2)$$

The covariance $\boldsymbol{\Sigma}_k$ ultimately depends on the environment features (e.g., it will be more elongated in the x direction if there are less features that allow to localize in that direction); as such, it is partly under the control of the user.

If the assumption does not hold, then it is recommended to use the technique of *covariance inflation*; this consists in neglecting the off-diagonal correlations, and "inflate" the diagonal elements[2]. This guarantees that the estimate found is still consistent (i.e., the estimated covariance is a conservative approximation of the actual covariance).

Algorithm overview: Our plan for solving the problem consists of the following steps, which will be detailed in the rest of the section.

- *A) Linear estimation of J_{21}, J_{22}.*
  We show that it is possible to solve for the parameters $J_{21} = -r_{\mathrm{L}}/b$, $J_{22} = r_{\mathrm{R}}/b$ independently of the others by considering only the rotation measurements $\hat{s}^k_\theta$. In fact, s^k_θ depends linearly on J_{21}, J_{22}, therefore the parameters can be recovered easily and robustly via linear least squares. This first part of the algorithm is equivalent to the procedure in Antonelli *et al.* [10], [11].
- *B) Nonlinear estimation of the other parameters.*
  - *1) Treatable approximation of the likelihood.*
    We show that, under Assumption 1, it is possible to write the term $||\hat{\boldsymbol{s}}^k - \ominus \boldsymbol{\ell} \oplus \boldsymbol{r}^k \oplus \boldsymbol{\ell}||$ in (10) as $||\boldsymbol{\ell} \oplus \hat{\boldsymbol{s}}^k - \boldsymbol{r}^k \oplus \boldsymbol{\ell}||$, which is easier to minimize.
  - *2) Integration of the kinematics.*
    We show that, given the knowledge of J_{21}, J_{22}, for any trajectory the translation (r^k_x, r^k_y) is a linear function of the wheel axis length b.
  - *3) Constrained quadratic optimization formulation.*
    We use the trick of considering $\cos \ell_\theta, \sin \ell_\theta$ as two separate variables. This allows writing the original objective function as a quadratic function of the vector $\boldsymbol{\varphi} = \begin{pmatrix} b & \ell_x & \ell_y & \cos \ell_\theta & \sin \ell_\theta \end{pmatrix}^T$, which contains all four remaining parameters. A constraint of the form $\varphi_4^2 + \varphi_5^2 = 1$ is added to ensure the consistency of the solution.
  - *4) Solution of the constrained quadratic system.*
    We show that the constrained quadratic problem can be solved in closed form; thus we can estimate the parameters $b, \ell_x, \ell_y, \ell_\theta$.
  - *5) Recovering $r_{\mathrm{L}}, r_{\mathrm{L}}$.*
    The radii are estimated from J_{21}, J_{22}, and b.

[2]For a 2×2 matrix, we substitute the matrix $\begin{pmatrix} \sigma_x^2 & \rho_{xy}\sigma_x\sigma_y \\ \rho_{xy}\sigma_x\sigma_y & \sigma_y^2 \end{pmatrix}$ with $\max(\sigma_x^2, \sigma_y^2) \left(\begin{smallmatrix} 1 & 0 \\ 0 & 1 \end{smallmatrix}\right)$.

C) Outlier removal.
An outlier detection/rejection phase must be integrated in the algorithm to deal with slipping and other sources of unmodeled errors.

D) Uncertainty estimation.
Finally, an estimate of the uncertainty of the solution can be computed using the Cramér–Rao bound.

A. Linear Estimation of J_{21}, J_{22}

The two parameters $J_{21} = -r_\mathrm{L}/b$ and $J_{22} = r_\mathrm{R}/b$ can be estimated by solving a weighted least squares problem. This subproblem is entirely equivalent to the procedure described in Antonelli *et al.* [10], [11].

Firstly, note that the constraint equation (9) implies that $s_\theta^k = r_\theta^k$: the robot and the sensor see the same rotation.

From the kinematics of the robot, we know that the rotational displacement of the robot is a linear function of the wheel velocities and the odometry parameters. More precisely, from (1–2), we have $r_\theta^k = \boldsymbol{L}_k \binom{J_{21}}{J_{22}}$, with $\boldsymbol{L}_k$ a row vector that depends on the velocities:

$$\boldsymbol{L}_k = \begin{pmatrix} \int_{t_k}^{t_{k+1}} \omega_\mathrm{L}(t)\,dt & \int_{t_k}^{t_{k+1}} \omega_\mathrm{R}(t)\,dt \end{pmatrix}. \tag{11}$$

Using the available estimate $\hat{s}_\theta^k$ of s_θ^k, with standard deviation σ_θ^k, an estimate of J_{21}, J_{22} can be found via linear least squares as

$$\begin{pmatrix} \hat{J}_{21} \\ \hat{J}_{22} \end{pmatrix} = \left[\sum_k \frac{\boldsymbol{L}_k^T \boldsymbol{L}_k}{\left(\sigma_\theta^k\right)^2} \right]^{-1} \sum_k \frac{\boldsymbol{L}_k^T}{\left(\sigma_\theta^k\right)^2} \hat{s}_\theta^k. \tag{12}$$

The matrix $\sum_k \boldsymbol{L}_k^T \boldsymbol{L}_k$ is invertible if the trajectories are exciting; otherwise, the problem is underconstrained.

B. Nonlinear estimation of the other parameters

We now assume that the parameters $J_{21} = -r_\mathrm{L}/b$ and $J_{22} = r_\mathrm{R}/b$ have already been estimated. The next step solves for the parameters b, $\ell_x, \ell_y, \ell_\theta$. When b is known, one can then recover $r_\mathrm{R}, r_\mathrm{L}$ from J_{21} and J_{22}.

1) Treatable likelihood approximation: The first step is simplifying the expression (10) for the log-likelihood. For the standard 2-norm, the following equivalence holds:

$$||\boldsymbol{s}^k - \ominus\boldsymbol{\ell} \oplus \boldsymbol{r}^k \oplus \boldsymbol{\ell}||_2 = ||\boldsymbol{\ell} \oplus \boldsymbol{s}^k - \boldsymbol{r}^k \oplus \boldsymbol{\ell}||_2.$$

Intuitively, the two vectors on the left and right hand side represent the same quantity in two different reference frames, so they have the same norm. This is not true for a generic matrix norm. However, it is true for the $\boldsymbol{\Sigma}_k^{-1}$-norm, which, thanks to Assumption 1 above is isotropic in the x and y directions, and hence rotation-invariant. Therefore, the log-likelihood (10) can be written as

$$\mathcal{J} = -\tfrac{1}{2} \sum_k ||\boldsymbol{\ell} \oplus \hat{\boldsymbol{s}}^k - \boldsymbol{r}^k \oplus \boldsymbol{\ell}||^2_{\boldsymbol{\Sigma}_k^{-1}}. \tag{13}$$

Algorithm 1 Simultaneous calibration of odometry and sensor parameters

1) Passively collect measurements over any sufficiently exciting trajectory.
2) For each interval, run the sensor displacement algorithm to obtain the estimates $\hat{\boldsymbol{s}}^k$.
   Each interval thus contributes the data sample
   $$\langle \hat{\boldsymbol{s}}^k, \omega_\mathrm{L}(t), \omega_\mathrm{R}(t) \rangle, \qquad t \in [t_k, t_{k+1}].$$
3) Repeat N times (for outlier rejection):
   Linear estimation of J_{21}, J_{22}:
   a) For all samples, compute the matrix $\boldsymbol{L}_k$ using (11).
   b) Form the matrix $\sum_k \boldsymbol{L}_k^T \boldsymbol{L}_k$. If the condition number of this matrix is over a threshold, declare the problem underconstrained and stop.
   c) Compute J_{21}, J_{22} using (12).
   Nonlinear estimation of the calibration parameters:
   d) For all samples, compute c_x^k, c_y^k (18–19) and $\boldsymbol{Q}_k$ using (20).
   e) Let $\boldsymbol{M} = \sum_k \boldsymbol{Q}_k^T \boldsymbol{Q}_k$.
   f) Compute the coefficients a, b, c using to (26–28) and find the two candidates $\lambda^{(1)}, \lambda^{(2)}$.
   g) For each $\lambda^{(i)}$:
      i) Compute the 5×5 matrix $\boldsymbol{N}^{(i)} = \boldsymbol{M} - \lambda^{(i)} \boldsymbol{W}$.
      ii) If the rank of $\boldsymbol{N}^{(i)}$ is less than 4, declare the problem underconstrained and stop.
      iii) Find a vector $\boldsymbol{\gamma}^{(i)}$ in the kernel of $\boldsymbol{N}^i$.
      iv) Compute $\boldsymbol{\varphi}^{(i)}$ using (29).
   h) Choose the optimal $\boldsymbol{\varphi}$ between $\boldsymbol{\varphi}^{(1)}$ and $\boldsymbol{\varphi}^{(2)}$ by computing the objective function.
   i) Compute the other parameters using (30).
   Outlier rejection:
   j) Compute the χ-value of each sample using (31).
   k) Discard a fraction α of the samples with the highest values of χ.

2) Integrating the kinematics: Let $\boldsymbol{r}(t) = \ominus\boldsymbol{q}^k \oplus \boldsymbol{q}(t)$, $t \geq t_k$, be the incremental robot displacement since the time t_k of the last exteroceptive observation. We need an explicit expression for $\boldsymbol{r}^k$ as a function of the parameters. We show that, if J_{21}, J_{22} are known, the displacement can be written as a linear function of the parameter b.

The displacement $\boldsymbol{r}(t)$ is the robot pose in a reference frame where the initial $\boldsymbol{q}^k$ is taken as the origin. It satisfies this differential equation with a boundary condition:

$$\dot{\boldsymbol{r}} = \begin{pmatrix} \dot{r}_x \\ \dot{r}_y \\ \dot{r}_\theta \end{pmatrix} = \begin{pmatrix} v\ \cos r_\theta \\ v\ \sin r_\theta \\ \omega \end{pmatrix}, \qquad \boldsymbol{r}(t_k) = \boldsymbol{0}. \tag{14}$$

The solution of this differential equation can be written explicitly as a function of the robot velocities. The solution for the rotation component r_θ is simply the integral of the angular velocity ω: $r_\theta(t) = \int_{t_k}^t \omega(\tau)\,d\tau$. Because $\omega = J_{21}\omega_\mathrm{L} + J_{22}\omega_\mathrm{R}$, the rotation component depends only on known quantities, therefore it can be estimated as

$$r_\theta(t) = \int_{t_k}^t \left(J_{21}\omega_\mathrm{L}(\tau) + J_{22}\omega_\mathrm{R}(\tau) \right)\,d\tau. \tag{15}$$

After $r_\theta(t)$ has been computed, the solution for the translation components r_x, r_y can be written as

$$r_x(t) = \int_{t_k}^{t} v(\tau)\,\cos\, r_\theta(\tau)\; d\tau, \tag{16}$$
$$r_y(t) = \int_{t_k}^{t} v(\tau)\,\sin\, r_\theta(\tau)\; d\tau. \tag{17}$$

Using the fact that $v = J_{11}\omega_{\mathrm{L}} + J_{12}\omega_{\mathrm{R}} = b(-\frac{1}{2}J_{21} + \frac{1}{2}J_{22})$, the final values $r_x^k = r_x(t_{k+1})$, $r_y^k = r_y(t_{k+1})$ can be written as a linear function of the unknown parameter b:

$$r_x^k = c_x^k\, b,$$
$$r_y^k = c_y^k\, b,$$

where the two constants c_x^k, c_y^k are a function of known data:

$$c_x^k = \tfrac{1}{2}\int_{t_k}^{t_{k+1}} \left(-J_{21}\omega_{\mathrm{L}}(\tau) + J_{22}\omega_{\mathrm{R}}(\tau)\right)\cos r_\theta^k(\tau)\; d\tau, \tag{18}$$
$$c_y^k = \tfrac{1}{2}\int_{t_k}^{t_{k+1}} \left(-J_{21}\omega_{\mathrm{L}}(\tau) + J_{22}\omega_{\mathrm{R}}(\tau)\right)\sin r_\theta^k(\tau)\; d\tau. \tag{19}$$

For a generic trajectory, three integrals are needed to find c_x^k, c_y^k (given by (15), (18), (19)); but if the wheel velocities are constant in the interval $[t_k, t_{k+1}]$, then a simplified closed form can be used, shown later in Section V-E.

3) Formulation as a quadratic system: We now use the trick of treating $\cos\ell_\theta$ and $\sin\ell_\theta$ as two independent variables. If we group the remaining parameters in the vector $\boldsymbol{\varphi} \in \mathbb{R}^5$ as

$$\boldsymbol{\varphi} = \begin{pmatrix} b & \ell_x & \ell_y & \cos\ell_\theta & \sin\ell_\theta \end{pmatrix}^T,$$

then (13) can be written as a quadratic function of $\boldsymbol{\varphi}$. More in detail, defining the 2×5 matrix $\boldsymbol{Q}_k$ of known coefficients as

$$\boldsymbol{Q}_k = \frac{1}{\sigma_{xy}^k}\begin{pmatrix} -c_x^k & 1-\cos\hat{r}_\theta^k & +\sin\hat{r}_\theta^k & +\hat{s}_x^k & -\hat{s}_x^k \\ -c_y^k & -\sin\hat{r}_\theta^k & 1-\cos\hat{r}_\theta^k & +\hat{s}_y^k & +\hat{s}_x^k \end{pmatrix}, \tag{20}$$

the log-likelihood function (13) can be written compactly as $-\frac{1}{2}\boldsymbol{\varphi}^T\boldsymbol{M}\boldsymbol{\varphi}$ + constant with $\boldsymbol{M} = \sum_k \boldsymbol{Q}_k^T\boldsymbol{Q}_k$. We have reduced the maximization of the likelihood to a quadratic problem with a quadratic constraint:

$$\min \quad \boldsymbol{\varphi}^T\boldsymbol{M}\boldsymbol{\varphi}, \tag{21}$$
$$\text{subject to} \quad \varphi_4^2 + \varphi_5^2 = 1. \tag{22}$$

Constraint (22), corresponding to $\cos^2\ell_\theta + \sin^2\ell_\theta = 1$, is necessary to enforce geometric consistency.

Note that so far the solution is not fully constrained: if the vector $\boldsymbol{\varphi}^\star$ is a solution of the problem, then $-\boldsymbol{\varphi}^\star$ is equally feasible and optimal. This phenomenon corresponds to the symmetry described by Proposition 4. To make the problem fully constrained, we add another constraint for $\boldsymbol{\varphi}$ that corresponds to choosing a positive axis b:

$$\varphi_1 \geq 0. \tag{23}$$

4) Solving the constrained least-squares problem: Because the objective function is bounded below, and the feasible set is closed, at least an optimal solution exists. We obtain optimality conditions using the method of Lagrange multipliers. The constraint (22) is written in matrix form as

$$\boldsymbol{\varphi}^T\boldsymbol{W}\boldsymbol{\varphi} = 1, \qquad \text{with } \boldsymbol{W} = \begin{pmatrix} \boldsymbol{0}_{3\times 3} & \boldsymbol{0}_{3\times 2} \\ \boldsymbol{0}_{2\times 3} & \boldsymbol{I}_{2\times 2} \end{pmatrix}. \tag{24}$$

Consider the Lagrangian $\mathcal{L} = \boldsymbol{\varphi}^T\boldsymbol{M}\boldsymbol{\varphi} + \lambda(\boldsymbol{\varphi}^T\boldsymbol{W}\boldsymbol{\varphi} - 1)$. In this problem, Slater's condition holds, thus the Karush–Kuhn–Tucker conditions are necessary for optimality:

$$\frac{\partial\mathcal{L}}{\partial\boldsymbol{x}}^T = 2\,(\boldsymbol{M} + \lambda\boldsymbol{W})\,\boldsymbol{\varphi} = \boldsymbol{0}. \tag{25}$$

Equation (25) implies that one needs to find a λ such that the matrix $(\boldsymbol{M} + \lambda\boldsymbol{W})$ is singular, and then find the solution $\boldsymbol{\varphi}$ in the kernel of such matrix. The value of λ can be found by solving the equation $\det(\boldsymbol{M} + \lambda\boldsymbol{W}) = 0$.

For an arbitrary $\boldsymbol{M}$, the expression $\det(\boldsymbol{M} + \lambda\boldsymbol{W})$ is a fifth-order polynomial in λ. However, the polynomial is only of the second order for the matrix $\boldsymbol{M} = \sum_k \boldsymbol{Q}_k^T\boldsymbol{Q}_k$, due to repeated entries in $\boldsymbol{Q}_k$. One can show that $\boldsymbol{M}$ has the following structure (note the zeros and repeated entries):

$$\boldsymbol{M} = \begin{pmatrix} m_{11} & 0 & m_{13} & m_{14} & m_{15} \\ & m_{22} & 0 & m_{35} & -m_{34} \\ & & m_{22} & m_{34} & m_{35} \\ & & & m_{44} & 0 \\ & \text{(symmetric)} & & & m_{44} \end{pmatrix}.$$

The determinant of $(\boldsymbol{M} + \lambda\boldsymbol{W})$ is a second-order polynomial $a_2\,\lambda^2 + a_1\,\lambda + a_0$, where the values of the coefficients can be computed as follows:

$$a_2 = m_{11}{m_{22}}^2 - m_{22}{m_{13}}^2, \tag{26}$$
$$\begin{aligned} a_1 = {} & 2m_{13}m_{22}m_{35}m_{15} - {m_{22}}^2{m_{15}}^2 + \\ & + 2m_{13}m_{22}m_{34}m_{14} - 2m_{22}{m_{13}}^2m_{44} - {m_{22}}^2{m_{14}}^2 + \\ & + 2m_{11}{m_{22}}^2m_{44} + {m_{13}}^2{m_{35}}^2 - 2m_{11}m_{22}{m_{34}}^2 + \\ & + {m_{13}}^2{m_{34}}^2 - 2m_{11}m_{22}{m_{35}}^2, \end{aligned} \tag{27}$$
$$\begin{aligned} a_0 = {} & -2m_{13}{m_{35}}^3m_{15} - m_{22}{m_{13}}^2{m_{44}}^2 + \\ & + {m_{13}}^2{m_{35}}^2m_{44} + 2m_{13}m_{22}m_{34}m_{14}m_{44} + \\ & + {m_{13}}^2{m_{34}}^2m_{44} - 2m_{11}m_{22}{m_{34}}^2m_{44} + \\ & - 2m_{13}{m_{34}}^3m_{14} - 2m_{11}m_{22}{m_{35}}^2m_{44} + \\ & + 2m_{11}{m_{35}}^2{m_{34}}^2 + m_{22}{m_{14}}^2{m_{35}}^2 + \\ & - 2m_{13}{m_{35}}^2m_{34}m_{14} - 2m_{13}{m_{34}}^2m_{35}m_{15} + \\ & + m_{11}{m_{34}}^4 + m_{22}{m_{15}}^2{m_{34}}^2 + \\ & + m_{22}{m_{35}}^2{m_{15}}^2 + m_{11}{m_{35}}^4 + m_{11}{m_{22}}^2{m_{44}}^2 + \\ & - {m_{22}}^2{m_{14}}^2m_{44} + 2m_{13}m_{22}m_{35}m_{15}m_{44} + \\ & + m_{22}{m_{34}}^2{m_{14}}^2 - {m_{22}}^2{m_{15}}^2m_{44}. \end{aligned} \tag{28}$$

The two candidate values $\lambda^{(1)}, \lambda^{(2)}$ for λ can be found in closed form as the roots of the second-order polynomial; one should examine both candidates, compute the corresponding vectors $\boldsymbol{\varphi}^{(1)}$, $\boldsymbol{\varphi}^{(2)}$, and check which one corresponds to the minimizer of the problem (21).

Let $\lambda^{(i)}$, $i = 1, 2$, be one of the two candidates. The 5×5 matrix $(\boldsymbol{M} + \lambda^{(i)}\boldsymbol{W})$ has rank *at most* 4 by construction. Under the excitability conditions discussed earlier, the rank is guaranteed to be exactly 4. In fact, otherwise we would be able to find a continuum of solutions for $\boldsymbol{\varphi}$, while the observability analysis guarantees the local uniqueness of the solution.

If the rank is 4, the kernel has dimension 1, and the choice of $\boldsymbol{\varphi}$ is unique given the constraints (9) and (23). Let $\boldsymbol{\gamma}^{(i)}$ be any non-zero vector in the kernel of $\left(\boldsymbol{M} + \lambda^{(i)}\boldsymbol{W}\right)$. To

obtain the solution $\boldsymbol{\varphi}^{(i)}$, scale $\boldsymbol{\gamma}^{(i)}$ by $\sqrt{(\gamma_4^{(i)})^2 + (\gamma_5^{(i)})^2}$ to enforce constraint (9), then flip it by the sign of γ_1^i to satisfy constraint (23):

$$\boldsymbol{\varphi}^{(i)} = \frac{\operatorname{sign}(\gamma_1^{(i)})}{\sqrt{(\gamma_4^{(i)})^2 + (\gamma_5^{(i)})^2}} \boldsymbol{\gamma}^{(i)}. \tag{29}$$

The correct solution $\hat{\boldsymbol{\varphi}}$ to (21) can be chosen between $\boldsymbol{\varphi}^{(1)}$ and $\boldsymbol{\varphi}^{(2)}$ by computing the value of the objective function. Given $\hat{\boldsymbol{\varphi}}$ and the previously estimated values of $\hat{J}_{21}, \hat{J}_{22}$, all six parameters can be recovered as follows:

$$\begin{aligned} \hat{b} &= \hat{\varphi}_1, \\ \hat{r}_{\mathrm{L}} &= -\hat{\varphi}_1 \hat{J}_{21}, \\ \hat{r}_{\mathrm{R}} &= +\hat{\varphi}_1 \hat{J}_{22}, \\ \hat{\boldsymbol{\ell}} &= (\hat{\varphi}_2, \hat{\varphi}_3, \operatorname{arctan2}(\hat{\varphi}_5, \hat{\varphi}_4)). \end{aligned} \tag{30}$$

C. Outlier removal

The practicality of our method comes from the fact that one can easily obtain thousands of observations by driving the robot, unattended, along arbitrary trajectories (compare, for example, with Borenstein's method, which is based on precise observation of a small set of data). Unfortunately, within thousands of observations, it is very likely that some are unusable, due to slipping of the wheels, failure of the sensor displacement estimation procedure, and the incorrect synchronization of sensor and odometry observations. In principle, a single outlier can drive the estimate arbitrarily far from the true value; formally, the *breakdown point* of a maximum likelihood estimator is 0. Thus an integral part of the algorithm is the outliers removal procedure, which consists in the classic strategy of progressively discarding a fraction of the samples that appear to be inconsistent [30].

Call a *sample* the set of measurements (wheel velocities, estimated sensor displacement) relative to the k-th interval. Samples are treated independently from each other, and the outlier removal procedure involves removing the samples that appear to be outliers, as follows.

Repeat N times:

1) Run the calibration procedure with the current samples.
2) Compute the χ–value of each sample as
$$\chi^k = ||\hat{\boldsymbol{s}}^k - \ominus\hat{\boldsymbol{\ell}} \oplus \boldsymbol{r}^k(\hat{r}_{\mathrm{L}}, \hat{r}_{\mathrm{R}}, \hat{b}) \oplus \hat{\boldsymbol{\ell}}||_{\boldsymbol{\Sigma}_k^{-1}}. \tag{31}$$
3) Discard a fraction α of the samples with the highest values of χ^k.

The parameters n and α depend, of course, on the properties of the data[3].

When implementing the method, examining the empirical distribution of the residual errors

$$\boldsymbol{e}^k = \hat{\boldsymbol{s}}^k - \ominus\hat{\boldsymbol{\ell}} \oplus \boldsymbol{r}^k(\hat{r}_{\mathrm{L}}, \hat{r}_{\mathrm{R}}, \hat{b}) \oplus \hat{\boldsymbol{\ell}} \tag{32}$$

gives precious information about the convergence of the estimation procedure. Ideally, if the estimation is accurate, $\boldsymbol{e}^k$ should be distributed according to the error model of the sensor displacement estimation procedure. For example, Fig. 3 shows the evolution of the residuals in one of the experiments to be presented later. We can see that in the first iteration (Fig. 3a) there are a few outliers; with every iteration, larger outliers are discarded, and because the estimate consequently improves, the residual distribution tends to be Gaussian shaped (Fig. 3b), with x, y errors the order of millimeters, and θ errors well below 1°.

[3] For example, in our experiments we used $N = 4$ and $\alpha = 0.01$, thus discarding about 5% of the data in total.

D. Uncertainty estimation

We use the Cramér–Rao bound (CRB) to estimate the uncertainty of the solution. Recall that the CRB is a lower bound on the attainable estimation accuracy. It can be shown that the maximum-likelihood estimator is *asymptotically* unbiased and attains the CRB [28]. If we have thousands of samples, we expect to be in the asymptotic regime of the maximum likelihood estimator.

The CRB is computed from the inverse of the Fisher Information Matrix (FIM), which depends on the observation model and the observation noise. Assuming a model of the kind $\boldsymbol{y}_k = \boldsymbol{f}_k(\boldsymbol{x}) + \boldsymbol{\epsilon}_k$, where $\boldsymbol{f}$ is differentiable, $\boldsymbol{x} \in \mathbb{R}^n$, $\boldsymbol{y} \in \mathbb{R}^m$ and $\boldsymbol{\epsilon}_k$ is Gaussian noise with covariance $\boldsymbol{\Sigma}_k$, the FIM is the $n \times n$ matrix given by $\boldsymbol{\mathcal{I}}(\boldsymbol{x}) = \sum_k \frac{\partial \boldsymbol{f}_k}{\partial \boldsymbol{x}} \boldsymbol{\Sigma}_k^{-1} \frac{\partial \boldsymbol{f}_k}{\partial \boldsymbol{x}}$. Under some technical conditions [28], the CRB states that any unbiased estimator $\hat{\boldsymbol{x}}$ of $\boldsymbol{x}$ is bounded by $\operatorname{cov}(\hat{\boldsymbol{x}}) \geq \boldsymbol{\mathcal{I}}(\boldsymbol{x})^{-1}$. In our case, the observations are $\boldsymbol{y}_k = \hat{\boldsymbol{s}}^k$, the state is $\boldsymbol{x} = (r_{\mathrm{R}}, r_{\mathrm{L}}, b, \ell_x, \ell_y, \ell_\theta)$ and the observation model $\boldsymbol{f}_k$ is given by (9), which is differentiated to obtain $\partial \boldsymbol{f}_k / \partial \boldsymbol{x}$.

E. Simpler formulas for constant wheel velocities

In Sections V-A and V-B we needed to integrate the kinematics to obtain some of the coefficients in the optimization problem. If the wheel velocities are constant within the time interval $[t_k, t_{k+1}]$, the formulas can be simplified.

If the robot velocities are constant ($v(t) = v_0$, $\omega(t) = \omega_0 \neq 0$), the solution of the differential equation (14) is

$$\boldsymbol{r}(t) = \begin{pmatrix} (v_0/\omega_0)\, \sin(\omega_0 t) \\ (v_0/\omega_0)\, (1 - \cos(\omega_0 t)) \\ \omega_0 t \end{pmatrix}. \tag{33}$$

For a proof, see for example [31, p. 516, formula (11.85)]. Let ω_{L}^k, ω_{R}^k be the constant wheel velocities during the k-th interval of duration $T^k = t_{k+1} - t_k$. Using (33), equation (11) can be simplified to

$$\boldsymbol{L}_k = \begin{pmatrix} T^k \omega_{\mathrm{L}}^k & T^k \omega_{\mathrm{R}}^k \end{pmatrix}, \tag{34}$$

and (18)-(19) are simplified to

$$r_\theta^k = J_{21} T^k \omega_{\mathrm{L}}^k + J_{22} T^k \omega_{\mathrm{R}}^k, \tag{35}$$

$$c_x^k = \tfrac{1}{2} T^k (-J_{21} \omega_{\mathrm{L}}^k + J_{22} \omega_{\mathrm{R}}^k) \frac{\sin(r_\theta^k)}{r_\theta^k}, \tag{36}$$

$$c_y^k = \tfrac{1}{2} T^k (-J_{21} \omega_{\mathrm{L}}^k + J_{22} \omega_{\mathrm{R}}^k) \frac{1 - \cos(r_\theta^k)}{r_\theta^k}. \tag{37}$$

Thus, if velocities are constant during each interval, one does not need to evaluate any integral numerically.

VI. Experiments

We tested the method using a Khepera III robot with an on-board Hokuyo URG-04LX range-finder. The experimental data and the software used are available as part of the supplemental materials[4].

A. Setup

1) Robot: The Khepera III is a small mobile robot suitable for educational use (Fig. 2). It has a diameter of 13 cm and a weight of 690 g. Brushless servo motors allow a maximum speed of 0.5 m/s. The Khepera III has an encoder resolution of about 7 ticks per degree. The Khepera's on-board CPU (DsPIC 30F5011 60 MhZ with the proprietary Korebot extension at 400 MhZ), is too slow to perform scan matching in real time because it does not possess a floating point unit: a scan matching operation that would take about 10 ms on a desktop computer takes about 10 s on the Khepera using floating point emulation. Therefore, the range-finder and odometry measurements are transmitted back to a desktop computer that runs the calibration procedure. Given the scan matching results $\hat{\boldsymbol{s}}^k$, the computational cost of the calibration algorithm in itself is negligible, and can be implemented on the Khepera, even with floating point emulation.

2) Sensors: The Hokuyo URG-04LX is a small lightweight range-finder sensor [32], [33]. It provides 681 rays over a 240 deg field of view, with a radial resolution of 1 mm, and a standard deviation of about 3 mm. The measurements are highly correlated, with every ray's error being correlated with its 3-4 neighbors: this is probably a symptom of some post-processing (interpolation) to bump up the resolution to the nominal 1024/360 rays/degrees. There is a bias exhibiting temporal drift: readings change as much as 20mm over a period of 5 minutes—this could be due to the battery power, or the change in temperature. There is also a spatial bias which is a function of the distance [32]: in practice, a rectangular environment appears slightly curved to the sensor. Notwithstanding these problems, we estimated the results of a scan matching operation to be accurate in the order of 1mm and tenths of degrees for small (5-10 cm) displacements.

[4]An up-to-date version of the software is also available at the website http://purl.org/censi/2011/calibration.

Figure 2. The Khepera III robot with an on-board Hokuyo URG-04LX range-finder used in the experiments.

3) Estimation of sensor displacement: To obtain the estimates $\hat{\boldsymbol{s}}^k$, we used the scan matching method described in [34].

There are various possible ways to estimate the covariance $\boldsymbol{\Sigma}_k$: either by using the knowledge of the internal workings of the scan matching method (e.g., [35]) or by using CRB-like bounds [36], which are independent of the algorithm, but assume the knowledge of an analytical model of the exteroceptive sensor.

Alternatively, if the robot has been collecting measurements in a uniform environment, so that it is reasonable to approximate the time-variant covariance $\boldsymbol{\Sigma}_k$ by a constant matrix $\boldsymbol{\Sigma}$, one can use the simpler (and more robust) method of identifying $\boldsymbol{\Sigma}$ directly from the data, by computing the covariance matrix of $\boldsymbol{e}^k$, after the solution has been obtained. This estimate is what is used in the following experiments.

4) Configurations: To test the method, we tried three configurations for the laser pose on the robot. This allows to check that the estimate for the odometry parameters remains consistent for a different configuration of the laser. We labeled the three configurations A, B, and C.

5) Trajectories: The method allows to use any trajectory, as long as it sufficiently excites all parameters. Practical considerations suggest to:

- Choose inputs that result in closed trajectories in a small confined space, so that the robot can run unattended.
- Choose piecewise-constant inputs. This allows to use the simplified formulas in Section V-E, and memorize only one value for ω_{L} and ω_{R} in one interval, instead of memorizing the entire profile $\omega_{\mathrm{L}}(t)$, $\omega_{\mathrm{R}}(t)$ for $t \in [t_k, t_{k+1}]$ which is necessary to use the formulas for the generic case.

In the experiments, we drive the robot according to trajectories that contain the four pairs of "canonical" inputs:

$$(\omega_{\mathrm{L}}, \omega_{\mathrm{R}}) = \pm c\,(+1, +1),$$
$$(\omega_{\mathrm{L}}, \omega_{\mathrm{R}}) = \pm c\,(+1, -1),$$
$$(\omega_{\mathrm{L}}, \omega_{\mathrm{R}}) = \pm c\,(+1, 0),$$
$$(\omega_{\mathrm{L}}, \omega_{\mathrm{R}}) = \pm c\,(0, +1).$$

The nominal trajectories associated to these inputs are elementary. In particular, the first input corresponds to a straight trajectory; the second to the robot turning in place; the last two to the motions originated by moving only one wheel. These trajectories are pieced together such that, at the end of each execution, the robot returns to the starting pose (up to drift); in this way, it is possible for the calibration procedure to run unattended in a confined space.

B. Numerical results

For each of the configurations A, B, C we collected several data logs using the aforementioned inputs. Then, we subdivided the data in 3 subsets for each configuration, named A_1, A_2, A_3, B_1, B_2, etc. In total, each subset was composed of about 3500 measurement samples.

For each configuration, we ran the calibration algorithm both on the complete data set, as well as on each subset

individually. Considering multiple subsets for the same configuration allows to check whether the uncertainty estimate is consistent: for example, we expect that the subsets A_1 and A_2 give slightly different calibration results, but those results must not disagree more than the estimated confidence bounds predict.

The results of calibration for the parameters are shown in Fig. 4. Subfigures 4a–4f show the estimates for the parameters r_{R}, r_{L}, b, ℓ_x, ℓ_y, ℓ_θ. Fig. 4g–4j show the same for the parameters J_{11}, J_{12}, J_{21}, J_{22}. The error bars correspond to the confidence values of 3σ given by the computation of the Cramér–Rao bound. The same data is shown in textual form in Table II.

The precision of the method is in the order of millimeters and tenths of degrees for the pose of the laser, and it is not possible for us to measure ground truth with such a precision. However, we can make the claim that the performance is very close to optimality using an indirect verification: by processing different subsets of the same logs, and verifying that the results agree on the level of confidence given by the associated Cramér–Rao bound. For example, in Fig. 4 we see that, although the estimates of r_{L} are different across the sets A_1, A_2, A_3, they are compatible with the confidence bounds. In the same way we can compare the estimates for ℓ_x, ℓ_y, ℓ_θ across each configuration.

Moreover, the estimates of the odometry parameters r_{R}, r_{L}, b (and the equivalent parametrization J_{11}, J_{12}, J_{21}, J_{22}) can also be compared across all three configurations A, B, C. For example, in Fig. 4g–4j we can see that, although the estimates of J_{11}, J_{12}, J_{21}, J_{22} change in each set, and the uncertainty varies much as well, all the data are coherent with the level of confidence given by the Cramér–Rao bound.

Note that the uncertainty (error bars) varies considerably across configurations, even though the number of measurements is roughly the same for each set. To explain this apparent inconsistency, one should recall that the confidence limits for a single variable give only a partial idea of the estimation accuracy; in fact, it is equivalent to considering only the diagonal entries of the covariance matrix, and neglecting the information about the correlation among variables. For example, the estimates of r_{L} and b are strongly positively correlated, because it is their ratio $J_{21} = r_{\mathrm{L}}/b$ that is directly observable.

In this case, there is a large correlation among the variables, and the correlation is influenced by the sensor pose configuration. This is shown in detail in Fig. 5 where the correlation patterns among all variables are presented. In Fig. 5b, we can see that having a displaced sensor introduces a strong correlation between ℓ_x, ℓ_y and ℓ_θ. Comparing Fig. 5a and 5c, we see that simply rotating the sensor does not change the correlation pattern.

VII. Conclusions

In this paper, we have presented a simple and practical method for simultaneously calibrating of the odometric parameters of a differential drive robot and the extrinsic pose of an exteroceptive sensor placed on the robot. The method has some interesting characteristics: it can run unattended, with no human intervention; no apparatus has to be calibrated a priori; there is no need for nominal parameters as an initial guess, as the globally optimal solution is found in a closed form; robot trajectories can be freely chosen, as long as they excite all parameters. We have experimentally evaluated the method on a mobile platform equipped with a laser range-finder placed in various configurations, using scan matching as the sensor displacement estimation method, and we have showed that the calibration accuracy is comparable to the theoretical limit given by the Cramér–Rao bound.

Among the possible evolutions of this work, we mention the simultaneous calibration problem for other kinematic models of mobile platforms, such as the car-like robot. Another interesting extension would be moving the problem to a dynamic setting, with a sensor that measures forces or accelerations.

References

[1] J. Doebbler, J. Davis, J. Junkins, and J. Valasek, "Odometry and calibration methods for multi-castor vehicles," in *Proceedings of the IEEE International Conference on Robotics and Automation*, pp. 2110–2115, May 2008.

[2] H. J. Von der Hardt, R. Husson, and D. Wolf, "An automatic calibration method for a multisensor system: application to a mobile robot localization system," in *Proceedings of the IEEE International Conference on Robotics and Automation*, vol. 4, (Leuven, Belgium), pp. 3141–3146, May 1998.

[3] J. Borenstein and L. Feng, "Measurement and correction of systematic odometry errors in mobile robots," *IEEE Transactions on Robotics and Automation*, vol. 12, December 1996.

[4] A. Kelly, "Fast and easy systematic and stochastic odometry calibration," in *Proceedings of the IEEE/RSJ International Conference on Intelligent Robots and Systems*, vol. 4, pp. 3188–3194, Sept./Oct. 2004.

[5] T. D. Larsen, M. Bak, N. A. Andersen, and O. Ravn, "Location estimation for an autonomously guided vehicle using an augmented Kalman filter to autocalibrate the odometry," in *First International Conference on Multisource-Multisensor Information Fusion (FUSION'98)*, 1998.

[6] D. Caltabiano, G. Muscato, and F. Russo, "Localization and self-calibration of a robot for volcano exploration," in *Proceedings of the IEEE International Conference on Robotics and Automation*, vol. 1, pp. 586–591, Apr./May 2004.

[7] A. Martinelli, N. Tomatis, and R. Siegwart, "Simultaneous localization and odometry self calibration for mobile robot," *Autonomous Robots*, vol. 22, pp. 75–85, 2006.

[8] E. Foxlin, "Generalized architecture for simultaneous localization, auto-calibration, and map-building," in *Proceedings of the IEEE/RSJ International Conference on Intelligent Robots and Systems*, vol. 1, pp. 527–533 vol.1, 2002.

[9] N. Roy and S. Thrun, "Online self-calibration for mobile robots," in *Proceedings of the IEEE International Conference on Robotics and Automation*, 1999.

[10] G. Antonelli, S. Chiaverini, and G. Fusco, "A calibration method for odometry of mobile robots based on the least-squares technique: theory and experimental validation," *IEEE Transactions on Robotics*, vol. 21, pp. 994–1004, Oct. 2005.

[11] G. Antonelli and S. Chiaverini, "Linear estimation of the physical odometric parameters for differential-drive mobile robots," *Autonomous Robots*, vol. 23, no. 1, pp. 59–68, 2007.

[12] G. Antonelli and S. Chiaverini, "A deterministic filter for simultaneous localization and odometry calibration of differential-drive mobile robots," in *Third European Conference on Mobile Robots*, 2007.

[13] Q. Zhang and R. Pless, "Extrinsic calibration of a camera and laser range finder (improves camera calibration)," in *Proceedings of the IEEE/RSJ International Conference on Intelligent Robots and Systems*, vol. 3, pp. 2301–2306, 2004.

[14] X. Brun and F. Goulette, "Modeling and calibration of coupled fish-eye ccd camera and laser range scanner for outdoor environment reconstruction," in *3DIM07*, pp. 320–327, 2007.

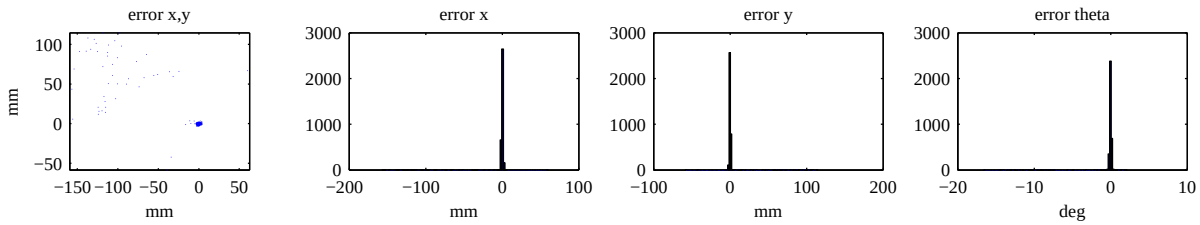

(a) Residuals after 1 iteration

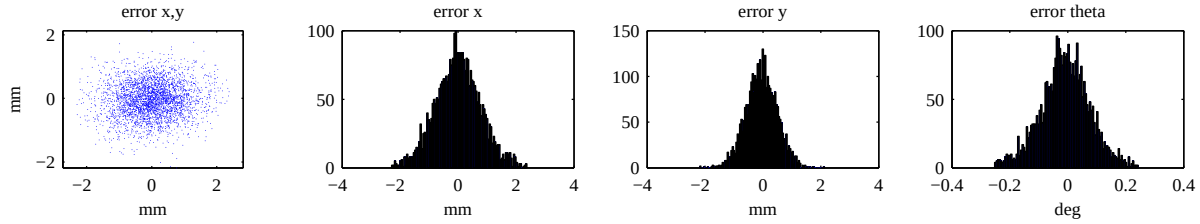

(b) Residuals after 4 iterations

Figure 3. Residuals distribution. An integral part of the method is the identification and removal of outliers, which may be due to wheel slipping, failure in the sensor displacement estimation procedure, and other unmodeled sources of noise. To identify outliers, one first performs calibration, and then computes the residual for each sample, according to equation (32). Samples with large residuals are discarded and the process is repeated. The distribution of residuals gives information about the quality of the estimate. (a): In the first iteration we expect large residuals. If the procedure is correct, the residuals should be ultimately distributed according to the sensor model. (b): In this case, we see that at the end of calibration the residuals are distributed according to the scan matching error process: approximately Gaussian, with a precision in the order of millimeters and fractions of a degree.

Table II
CALIBRATED PARAMETERS AND CONFIDENCE INTERVALS
(THE SAME INFORMATION IS PRESENTED IN GRAPHICAL FORM IN FIG. 4.)

	r_{L} (mm)	r_{R} (mm)	b (mm)	ℓ_x (mm)	ℓ_y (mm)	ℓ_θ (deg)
A	41.48 ± 0.37	41.67 ± 0.38	88.55 ± 1.60	-2.54 ± 1.40	6.08 ± 0.86	-89.06 ± 1.70
A_1	41.18 ± 0.80	41.35 ± 0.81	87.86 ± 3.44	-2.41 ± 2.89	6.12 ± 1.82	-89.21 ± 3.56
A_2	41.56 ± 0.60	41.74 ± 0.60	88.68 ± 2.56	-2.34 ± 2.41	5.95 ± 1.37	-89.04 ± 2.91
A_3	41.65 ± 0.53	41.86 ± 0.54	89.00 ± 2.28	-2.82 ± 1.99	6.14 ± 1.21	-89.10 ± 2.41
B	41.41 ± 0.52	41.58 ± 0.50	88.36 ± 2.18	-6.02 ± 2.10	-38.39 ± 1.18	-106.63 ± 2.00
B_1	41.39 ± 0.87	41.55 ± 0.85	88.26 ± 3.67	-5.82 ± 3.70	-38.57 ± 1.97	-106.53 ± 3.53
B_2	41.44 ± 0.90	41.58 ± 0.87	88.36 ± 3.77	-6.27 ± 3.51	-38.24 ± 2.04	-106.96 ± 3.33
B_3	41.40 ± 0.90	41.58 ± 0.87	88.40 ± 3.77	-5.89 ± 3.61	-38.19 ± 2.03	-106.38 ± 3.45
C	41.86 ± 0.10	42.00 ± 0.10	89.25 ± 0.44	-6.04 ± 0.20	0.27 ± 0.24	0.53 ± 0.24
C_1	42.14 ± 0.17	42.25 ± 0.17	89.85 ± 0.74	-6.00 ± 0.48	0.40 ± 0.40	0.31 ± 0.57
C_2	41.61 ± 0.59	41.75 ± 0.59	88.64 ± 2.52	-6.27 ± 0.72	-0.15 ± 1.35	0.48 ± 0.86
C_3	41.77 ± 0.11	41.92 ± 0.11	89.13 ± 0.46	-5.94 ± 0.13	0.48 ± 0.24	0.81 ± 0.15

	J_{11} (mm/s)	J_{12} (mm/s)	J_{21} (deg/s)	J_{22} (deg/s)
A	10.37 ± 0.09	10.42 ± 0.09	-13.42 ± 0.13	13.48 ± 0.13
A_1	10.30 ± 0.20	10.34 ± 0.20	-13.43 ± 0.27	13.48 ± 0.27
A_2	10.39 ± 0.15	10.44 ± 0.15	-13.43 ± 0.20	13.48 ± 0.20
A_3	10.41 ± 0.13	10.46 ± 0.13	-13.41 ± 0.18	13.47 ± 0.18
B	10.35 ± 0.13	10.39 ± 0.13	-13.43 ± 0.17	13.48 ± 0.17
B_1	10.35 ± 0.22	10.39 ± 0.21	-13.43 ± 0.29	13.48 ± 0.29
B_2	10.36 ± 0.22	10.40 ± 0.22	-13.43 ± 0.29	13.48 ± 0.30
B_3	10.35 ± 0.22	10.40 ± 0.22	-13.42 ± 0.29	13.48 ± 0.30
C	10.47 ± 0.03	10.50 ± 0.03	-13.44 ± 0.03	13.48 ± 0.03
C_1	10.54 ± 0.04	10.56 ± 0.04	-13.44 ± 0.06	13.47 ± 0.06
C_2	10.40 ± 0.15	10.44 ± 0.15	-13.45 ± 0.19	13.49 ± 0.19
C_3	10.44 ± 0.03	10.48 ± 0.03	-13.43 ± 0.04	13.48 ± 0.04

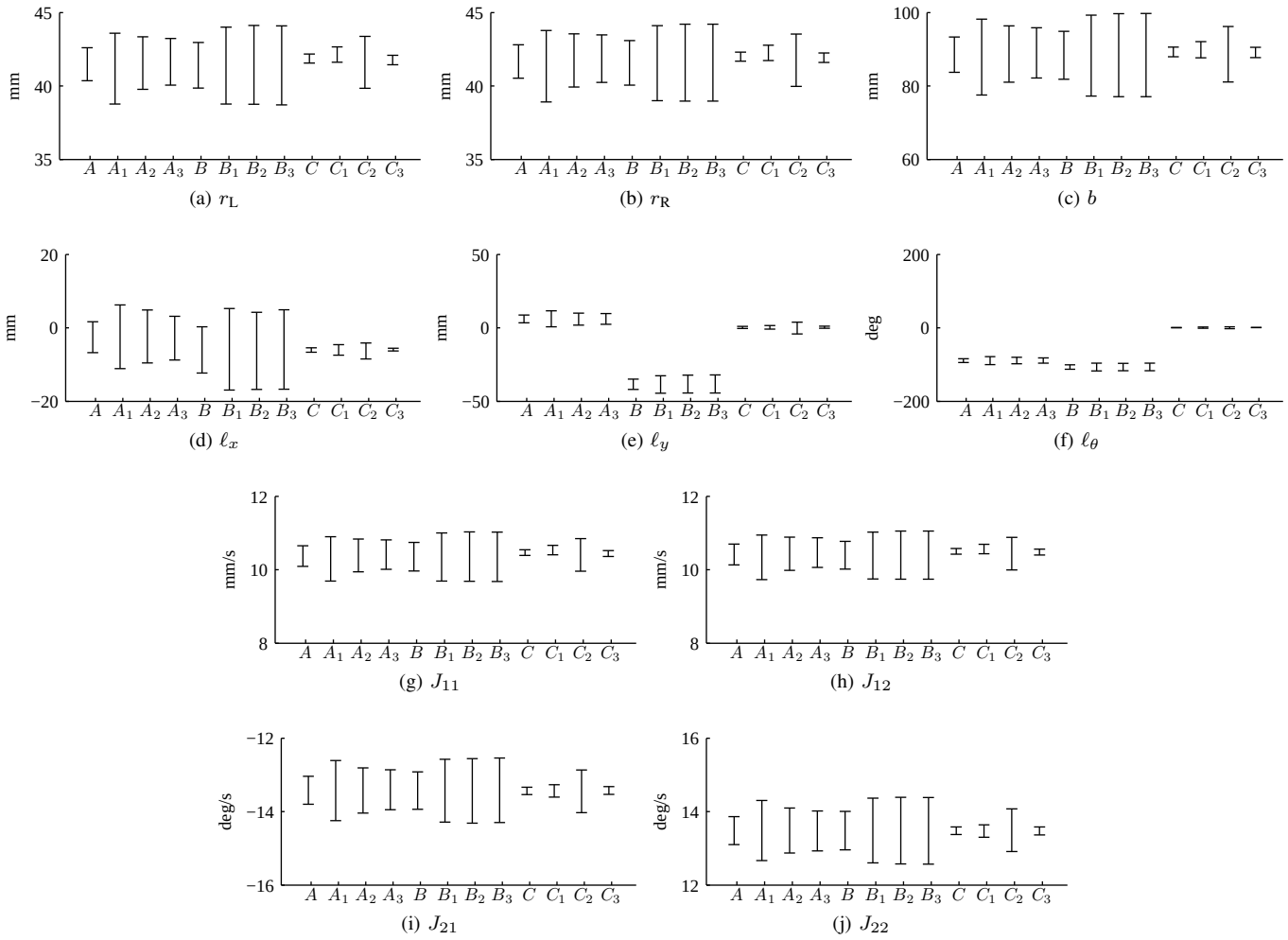

Figure 4. Calibrated parameters and confidence intervals (the same information is presented in tabular form in Table II). For each configuration, three logs are taken and considered separately (for example, A_1,A_2,A_3) and all together ("A"). Thus we have 12 datasets in total. On the x-axis we find the experiment label; on the y axis, the estimated value, along with 3σ confidence bars. The confidence bars correspond to the absolute achievable accuracy as computed by the Cramér–Rao bound, as explained in Section V-D. Note that most variables are highly correlated, therefore plotting only the standard deviations might be misleading; see Fig. 5 for more information about the correlation.

	r_{L}	r_{R}	b	ℓ_x	ℓ_y	ℓ_θ	J_{11}	J_{12}	J_{21}	J_{22}
J_{22}										
J_{21}										−.97
J_{12}									+.95	−.92
J_{11}								+.95	+.91	−.96
ℓ_θ							+.01	+.01	+.01	−.02
ℓ_y						−.09	−.03	+.01	+.02	+.01
ℓ_x					+.02	−.14	−.01	−.01	−.01	−.00
b				−.01	−.00	+.01	+.97	+.97	+.97	−.98
r_{R}			+.97	−.01	+.01	+.01	+.95	+.99	+.95	−.92
r_{L}		+.95	+.97	−.01	−.03	+.01	+.99	+.95	+.91	−.96

(a) Correlation pattern (configuration A)

	r_{L}	r_{R}	b	ℓ_x	ℓ_y	ℓ_θ	J_{11}	J_{12}	J_{21}	J_{22}
J_{22}										
J_{21}										−.97
J_{12}									+.96	−.94
J_{11}								+.96	+.93	−.97
ℓ_θ							−.24	−.25	−.24	+.22
ℓ_y						−.18	−.00	+.03	−.00	+.02
ℓ_x					−.30	+.63	−.15	−.16	−.16	+.14
b				−.16	−.00	−.24	+.98	+.98	+.98	−.99
r_{R}			+.98	−.16	+.03	−.25	+.96	+.99	+.96	−.94
r_{L}		+.96	+.98	−.15	−.00	−.24	+.99	+.96	+.93	−.97

(b) Correlation pattern (configuration B)

	r_{L}	r_{R}	b	ℓ_x	ℓ_y	ℓ_θ	J_{11}	J_{12}	J_{21}	J_{22}
J_{22}										
J_{21}										−.99
J_{12}									+.98	−.97
J_{11}								+.98	+.96	−.99
ℓ_θ							−.01	−.01	−.01	−.00
ℓ_y						−.11	−.01	+.01	+.01	−.00
ℓ_x					−.01	−.01	−.00	−.00	−.01	−.00
b				−.01	−.00	−.01	+.99	+.99	+.99	−.99
r_{R}			+.99	−.00	+.01	−.01	+.98	+.99	+.98	−.97
r_{L}		+.98	+.99	−.00	−.01	−.01	+.99	+.98	+.96	−.99

(c) Correlation pattern (configuration C)

Figure 5. Correlation patterns between estimation errors. Fig. 4 shows the confidence intervals as 3σ error bars on each variable. That corresponds to considering only the diagonal elements of the covariance matrix and neglecting the correlation information. As it turns out, each configuration has a typical correlation pattern, which critically describes the overall accuracy. Subfigures (a), (b), (c) show the correlation patterns for the three configurations A, B, C. Each cell in the grid contains the correlation between the two variables on the axes.

[15] H. Aliakbarpour, P. Nuez, J. Prado, K. Khoshhal, and J. Dias, "An efficient algorithm for extrinsic calibration between a 3d laser range finder and a stereo camera for surveillance," in *International Conference on Advanced Robotics (ICAR)*, pp. 1–6, June 2009.

[16] A. Martinelli and D. Scaramuzza, "Automatic self-calibration of a vision system during robot motion," in *Proceedings of the IEEE International Conference on Robotics and Automation*, (Orlando, Florida), 2006.

[17] A. Martinelli and R. Siegwart, "Observability properties and optimal trajectories for on-line odometry self-calibration," in *45th IEEE Conference on Decision and Control*, pp. 3065–3070, Dec. 2006.

[18] F. Mirzaei and S. Roumeliotis, "A kalman filter-based algorithm for imu-camera calibration: Observability analysis and performance evaluation," *IEEE Transactions on Robotics*, vol. 24, pp. 1143–1156, Oct. 2008.

[19] J. Hesch, A. Mourikis, and S. Roumeliotis, "Determining the camera to robot-body transformation from planar mirror reflections," in *Proceedings of the IEEE/RSJ International Conference on Intelligent Robots and Systems*, pp. 3865–3871, Sept. 2008.

[20] J. P. Underwood, A. Hill, T. Peynot, and S. J. Scheding, "Error modeling and calibration of exteroceptive sensors for accurate mapping applications," *Journal of Field Robotics*, vol. 27, pp. 2–20, Jan. 2010.

[21] J. Brookshire and S. Teller, "Automatic Calibration of Multiple Coplanar Sensors," in *Proceedings of Robotics: Science and Systems (RSS)*, 2011.

[22] A. Censi, L. Marchionni, and G. Oriolo, "Simultaneous maximum-likelihood calibration of robot and sensor parameters," in *Proceedings of the IEEE International Conference on Robotics and Automation*, (Pasadena, CA), May 2008.

[23] A. Martinelli, "Local decomposition and observability properties for automatic calibration in mobile robotics," in *Proceedings of the IEEE International Conference on Robotics and Automation*, pp. 4182–4188, May 2009.

[24] A. Martinelli, "State Estimation Based on the Concept of Continuous Symmetry and Observability Analysis: The Case of Calibration," *IEEE Transactions on Robotics*, vol. 27, no. 2, pp. 239–255, 2011.

[25] G. Antonelli, F. Caccavale, F. Grossi, and A. Marino, "A non-iterative and effective procedure for simultaneous odometry and camera calibration for a differential drive mobile robot based on the singular value decomposition," *Intelligent Service Robotics*, vol. 3, pp. 163–173, June 2010.

[26] R. M. Murray, Z. Li, and S. S. Sastry, *A Mathematical Introduction to Robotic Manipulation*. CRC, 1 ed., March 1994.

[27] R. Hermann and A. Krener, "Nonlinear controllability and observability," *IEEE Transactions on Automatic Control*, vol. 22, pp. 728–740, Oct 1977.

[28] H. L. V. Trees and K. L. Bell, *Bayesian Bounds for Parameter Estimation and Nonlinear Filtering/Tracking*. Wiley-IEEE Press, 2007.

[29] S. Boyd and L. Vandenberghe, *Convex Optimization*. New York, NY, USA: Cambridge University Press, 2004.

[30] P. J. Rousseeuw and A. M. Leroy, *Robust regression and outlier detection (3rd edition)*. John Wiley & Sons, 1996.

[31] B. Siciliano, L. Villani, L. Sciavicco, and G. Oriolo, *Robotics: Modelling, Planning and Control*. Springer, 2008.

[32] H. Kawata, A. Ohya, S. Yuta, W. Santosh, and T. Mori, "Development of ultra-small lightweight optical range sensor system," in *Proceedings of the IEEE/RSJ International Conference on Intelligent Robots and Systems*, pp. 1078–1083, Aug. 2005.

[33] L. Kneip, F. T. G. Caprari, and R. Siegwart, "Characterization of the compact hokuyo URG-04LX 2d laser range scanner," in *Proceedings of the IEEE International Conference on Robotics and Automation*, (Kobe, Japan), 2009.

[34] A. Censi, "An ICP variant using a point-to-line metric," in *Proceedings of the IEEE International Conference on Robotics and Automation*, pp. 19–25, May 2008. Source code available at http://andreacensi.github.com/csm/. Also available as a ROS package at http://www.ros.org/wiki/laser_scan_matcher.

[35] A. Censi, "An accurate closed-form estimate of ICP's covariance," in *Proceedings of the IEEE International Conference on Robotics and Automation*, (Rome, Italy), pp. 3167–3172, Apr. 2007.

[36] A. Censi, "On achievable accuracy for pose tracking," in *Proceedings of the IEEE International Conference on Robotics and Automation*, (Kobe, Japan), pp. 1–7, May 2009.